Geochemical Perspectives Letters

$Fe(II)_{aq}$-induced transformation of Fe-rich precipitates from a hydrothermal field

Z. Zhou, J. Li, L. Notini, Z. He, M. Schad, K.O. Konhauser, S. Yang

Supplementary Information

The Supplementary Information includes:

- Supplementary Methods
- Tables S-1 to S-3
- Figures S-1 to S-4
- Supplementary Information References

Supplementary Methods

1. Sequential Fe Extractions

The extractions were conducted in a glovebox filled with N_2 (O_2 < 0.2 ppm). Triplicate reactors were sampled in regular intervals over 14 days of reaction. At each time point, aliquots were centrifuged, the supernatant filtered (0.22 µm) and subsequently acidified with HCl to preserve the Fe(II) in ~0.1 M HCl. The solids were subjected to sequential extractions under anoxic conditions using 1 M $MgCl_2$ (exchangeable Fe pool), 0.5 M HCl (amorphous to poorly crystalline Fe oxyhydroxides), and finally the residual solids were dissolved in 6 M HCl under microwave for 15 seconds (Voelz *et al.*, 2019). The concentrations of Fe(II) and total Fe in the aqueous, exchangeable, 0.5 M HCl extractable, and 6 M HCl extractable pools were analysed with a modified ferrozine method (Viollier *et al.*, 2000).

2. Fe Isotope Measurement

For Fe isotope composition, samples were diluted with 2% HNO_3 (double distilled) to achieve a final Fe concentration of ~2 µM, and analyzed using a quadrupole ICP-MS (Agilent 7900). He gas mode with a collision cell was applied to remove isobaric interferences with Argon (primarily $^{40}Ar^{16}O$ and $^{40}Ar^{16}O^{1}H$) for ^{56}Fe and ^{57}Fe (Zhou *et al.*, 2018). Four Fe isotopes (^{54}Fe, ^{56}Fe, ^{57}Fe, and ^{58}Fe) were measured, and the percent of ^{57}Fe in each sample was calculated as an indicator for Fe isotope mixing processes. Fe isotope standards (2.1 % and 96.0 % of ^{57}Fe) and internal standards of ^{103}Rh and ^{115}In were used to monitor instrument stability and correct between samples. The measurement precision of ^{57}Fe percent was about 0.1 %.

3. Mineral Characterization

For SEM, the samples were coated with Au and operated at 5–30 kV with a maximum beam current of 200nA. An energy dispersive X-ray spectrometer (EDS) was used to identify elemental compositions. The TEM was equipped with a Schottky gun operating at 200 kV (Cs 1.0 mm, Cc 1.1 mm, point resolution of 1.9 Å). XRD patterns were collected from 5-80° with a step increment of 0.02° (tube conditions: 40 kV, 40 mA; Cu source), and processed using MDI JADE 6.0. The relative peak intensities of lepidocrocite and goethite, as well as the full-width at half maximum (FWHM) of identical peaks, were analysis and verified by full-pattern fitting using Rietveld refinements. Samples were further analysed by 57Fe Mössbauer Spectroscopy (Wissel GmbH, Germany) at the East China Normal University. Mössbauer spectra were collected at 295 K using a 57Co source in a Rh lattice and calibrated against an α-Fe(0) foil. Spectral fitting was performed using the Recoil software (University of Ottawa, Canada) with an extended Voigt-Based fitting (xVBF) routine. The phase interpretations were based on established fitting parameters (Vandenberghe and De Grave, 2013).

Supplementary Tables

Table S-1 Major and trace element composition of the precipitate used in this study. The precipitate was digested by 6M HCl, which was strong enough to total dissolve the solid based on our pre-test.

Element	Na	Mg	Al	K	Ca	Fe	Li	Sc	Ti	V	Cr	Mn
			(%)						(ppm)			
Weight fraction	0.17	0.52	0.07	0.00	0.72	50.08	15.63	3.47	381.94	39.93	BDL*	BDL*

Element	Co	Ni	Cu	Zn	Ga	Rb	Sr	Mo	Cd	Ba	Nd	U
						(ppm)						
Weight fraction	24.31	13.89	2710.07	793.40	3.47	8.68	31.25	85.07	6.94	10.42	6.94	13.89

*Below detection limit.

Table S-2 The FWHM value of representative identical peaks in different samples.

Face	Full-width at half maximum (FWHM)		
	Control	Reacted in HEPES	Reacted in ASW
Goethite [110]	0.905	0.715	0.893
Lepidocrocite [200]	0.262	-	0.320

Table S-3 Fitting parameters for ^{57}Fe Mössbauer spectra of different samples.

Sample	Phase	Phase interpretation	Area %	Center shift (mm s^{-1})	QS or Ɛ [a] (mm s^{-1})	Hyperfine field (T)	σ[b] (mm s^{-1}) or (T)	Red-χ^2
Control	Fe(III)-D1	Paramagnetic Fe(III) phases, likely Fh, Lp and nGt	82.3	0.37	0.60	-	0.17	0.65
	Fe(III)-S1	Likely goethite	17.7	0.38	-0.12	24.00	4.00	
Reacted in HEPES	Fe(II)-D1	Paramagnetic Fe(III) phases, likely Fh, and nGt	6.1	0.37	0.51	-	0.24	1.57
	Fe(III)-S2	Magnetite (Tetrahedral)	4.8	0.26	0.04	48.00	1.20	
	Fe(III)Fe(II)-S3	Magnetite (Octahedral)	5.8	0.67	-0.04	45.00	2.00	
	Fe(III)-S1	Likely goethite	83.3	0.38	-0.12	24.52	9.61	
Reacted in ASW	Fe(III)-D1	Paramagnetic Fe(III) phases, likely Fh, Lp and nGt	30.9	0.37	0.58	-	0.15	2.18
	Fe(III)-S1	Likely goethite	69.1	0.37	-0.06	17.30	10.46	

[a]Quadrupole splitting (QS, for doublets) or quadrupole shift (Ɛ, for sextets);
[b]σ, standard deviation of QS (doublet) or H (sextet);
Abbreviations: Fe(III)-D= Fe(III) doublet; Fe(III)-S = Fe(III) sextet; Fe(II)-D = Fe(II) doublet. Fh = ferrihydrite; Lp = lepidocrocite; nGt = nano goethite.

Supplementary Figures

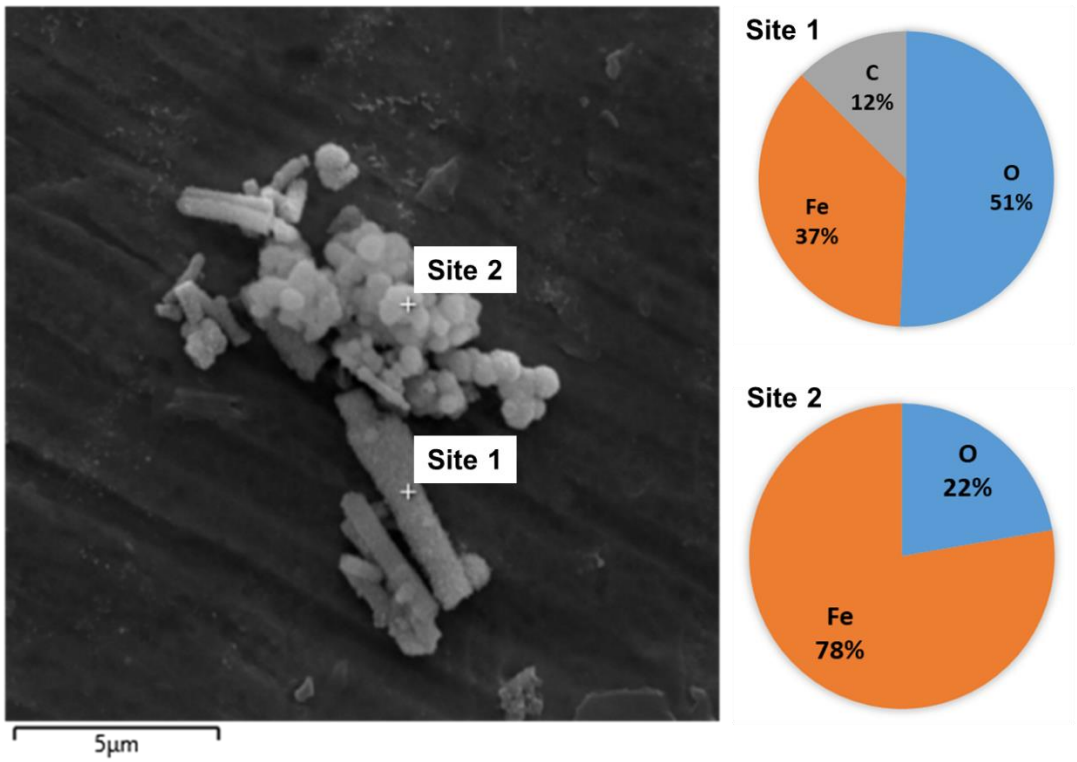

Figure S-1 Main elemental compositions of specific sites on typical structures of the original Fe-rich precipitates based on EDS results. No obvious Si signal (<1%) was identified.

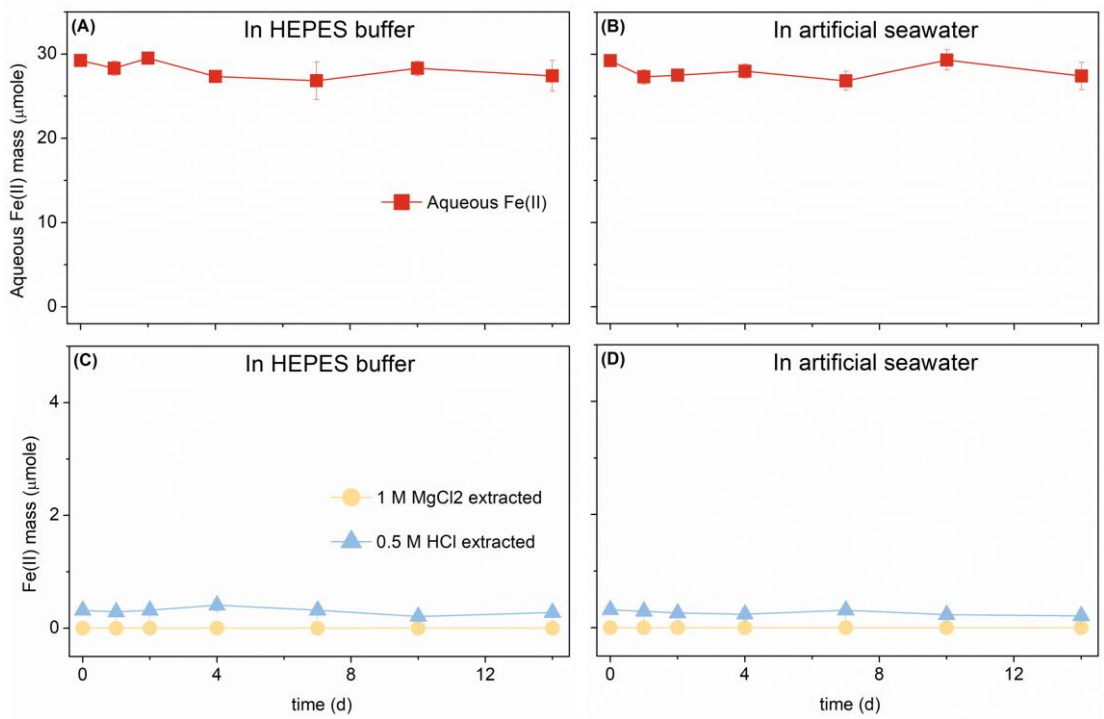

Figure S-2 $Fe(II)_{aq}$ control in (A) HEPES buffer and (B) artificial seawater, as well as the control groups with only the precipitates in (A) HEPES buffer and (B) artificial seawater. Each point represents the mean ± standard deviation of duplicate reactors. Where error bars are not visible, they are smaller than the symbols.

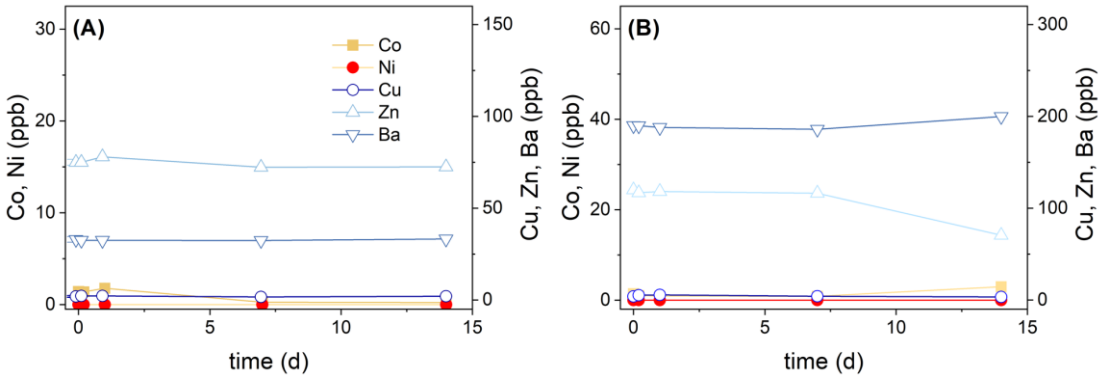

Figure S-3 Aqueous concentrations of Co, Ni (left Y axis) and Cu, Zn, Ba (right Y axis) in the Fe-rich precipitation control (without Fe(II)) in (A) HEPES buffer, and (B) artificial seawater.

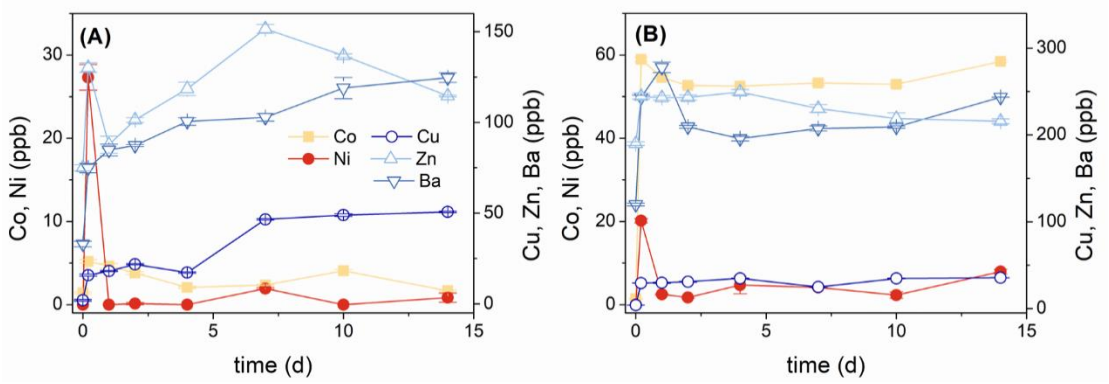

Figure S-4 The concentrations of trace metals in the aqueous phase during the reactions between $Fe(II)_{aq}$ and the precipitates in (A) HEPES buffer, and (B) artificial seawater. Each data point represents the mean ± standard deviation of triplicate reactors.

Supplementary Information References

Vandenberghe, R.E., De Grave, E. (2013) Application of Mössbauer Spectroscopy in Earth Sciences. In: Yoshida, Y., Langouche, G. (Eds.) *Mössbauer Spectroscopy: Tutorial Book*. Springer, Berlin Heidelberg, 91–185. https://doi.org/10.1007/978-3-642-32220-4_3

Viollier, E., Inglett, P., Hunter, K., Roychoudhury, A., Van Cappellen, P. (2000) The ferrozine method revisited: Fe (II)/Fe (III) determination in natural waters. *Applied geochemistry* 15, 785–790. https://doi.org/10.1016/S0883-2927(99)00097-9

Voelz, J.L., Johnson, N.W., Chun, C.L., Arnold, W.A., Penn, R.L. (2019) Quantitative Dissolution of Environmentally Accessible Iron Residing in Iron-Rich Minerals: A Review. *ACS Earth and Space Chemistry* 3, 1371–1392. https://doi.org/10.1021/acsearthspacechem.9b00012

Zhou, Z., Latta, D.E., Noor, N., Thompson, A., Borch, T., Scherer, M.M. (2018) Fe (II)-Catalyzed Transformation of Organic Matter–Ferrihydrite Coprecipitates: A Closer Look Using Fe Isotopes. *Environmental Science & Technology* 52, 11142–11150. https://doi.org/10.1021/acs.est.8b03407